Acc. Chem. Res. **2002,** *35,* 1079−1086

Chemical Doping of Single-Wall Carbon Nanotubes

JOHN E. FISCHER*

Department of Materials Science and Engineering, University of Pennsylvania, Philadelphia, Pennsylvania 19104-6272

Received February 20, 2002

ABSTRACT

Single-wall carbon nanotubes can be doped, or intercalated, with electron donors or acceptors, similar to graphite and some conjugated polymers. The resulting materials show many of the same features: enhanced electrical conductivity, conduction electron paramagnetism, partial or complete reversibility, and cyclability. Reactions may be carried out in vapor or liquid phase, or electrochemically. Structural information is sketchy at best, due to the limited quality of currently available materials and solvent-related effects. Recent developments in coagulation-based fiber extrusion and partially aligned materials offer new opportunities for novel material modifications by chemical doping.

Historical Context, Concepts, and Strategies

A few years after the discovery of carbon nanotubes by Iijima,[1] Smalley's group found that the single-wall variety (SWNT) self-assembled during growth into partially ordered two-dimensional bundles, or "ropes".[2] The large one-dimensional trigonal channels between tubes immediately suggested the possibility that ropes might afford a new carbon host lattice for intercalation, and that the reaction would likely be accompanied by charge exchange between host and guest. It appeared that the crystal chemistry of such phases would be similar to that of graphite intercalation compounds (GICs) and alkali fullerides. On the other hand, the dimensionality corresponded more closely to that of doped crystalline conjugated polymers, except with weak van der Waals intertube bonding rather than the generally stronger interchain hydrogen bonding typical of crystalline polymers.[3,4] If they existed, SWNT intercalation compounds would form a new class of quasi-one-dimensional synthetic metals with the added benefit of very high strength. Furthermore, the possibility of "tuning" the chemical potential into one of the van Hove singularities characteristic of the SWNT electronic spectrum suggested opportunities for novel quasi-1D superconductors. Finally, if SWNT could be reversibly intercalated electrochemically, new opportunities for energy storage materials would be at hand.[3] In principle, the interior lumen of the nanotube affords an entirely new kind of site for adding foreign atoms or molecules, but this is accessible only by first applying an oxidative treatment to remove the fullerenic end-caps, introduce sidewall defects of sufficient size, and shorten the tubes so that the lumen will fill on a reasonable time scale.

Figure 1 shows schematically how an ideal SWNT crystal might fit into the pantheon of carbon-based, redox-derived salts. If this is the correct paradigm, we need to address two issues straightaway: the maximum guest concentration (limited by ionic repulsion) and the likelihood of finding first-order "staging" transitions vs concentration or chemical potential. We considered three models, shown in Figure 2, to estimate the maximum guest concentration.[5] The first is borrowed from what we know about polyacetylene $(CH)_x$ and (poly)paraphenylene-vinylene (PPV),[6] in which alkali dopants form monatomic interstitial chains. Filling all SWNT channels with touching spheres of K^+ gives only KC_{40}, a rather low limiting concentration. The second model is inspired by sodium fullerides[7] in which the large octahedral site in fcc C_{60} can accommodate as many as nine Na^+ ions. Assuming three chains per channel and allowing for a small lattice dilation, we get $\sim KC_{13}$. The third model resembles GICs, assuming that each tube surface is decorated with a cylindrically wrapped 2×2 commensurate superlattice as in KC_8 (Figure 1), thus fixing the composition at precisely this value. For this model, substantial lattice dilation would be required to minimize Coulomb repulsion among decorated tubes. Structure factor calculations show that all three models have unique signatures in X-ray diffraction.[5]

Staging in graphite and polymers refers to the cascade of definite compounds encountered as the guest concentration increases from zero to its maximum value. In the layer compounds, these are stabilized at low temperature by competition between interlayer repulsion and intralayer attraction.[8] The energy-minimizing configurations are long-period sequences of filled and empty van der Waals "galleries", the period being set by the external chemical potential μ. At high temperature, entropy dominates, and we have a three-dimensional lattice gas with partial filling of all galleries. Similar cascades, and the attendant first-order transitions, occur in doped polymers via a sequence of two-dimensional superlattices.[9] In both cases, the phase evolution vs T and μ is qualitatively accounted for by a one-dimensional Ising model in which the two spin states per site are replaced by a continuously variable gallery or channel filling.

How does this apply to SWNT ropes? In layer compounds, the origin of the intralayer attraction is believed to be dipole−dipole interactions between local deformations of the host layer induced by isolated guest atoms.[8] This conjecture is supported by the following observations. Graphite is easily deformable normal to the layer, and

John E. Fischer received his first degree in mechanical engineering from Rensselaer Polytechnic Institute in 1961, followed by a M.S. from the California Institute of Technology in 1962. He returned to RPI and obtained his Ph.D. in nuclear science and engineering in 1966, working with John Corelli. After a postdoctoral year in the Laboratoire de Physique at Ecole Normale Supérieure in Paris, he was a research physicist at Michelson Laboratory in China Lake, CA, from 1967 to 1973. He joined the University of Pennsylvania, where he is presently Professor of Materials Science and Engineering, in 1973. He has also held visiting positions at the Ecole Normale Supérieure, the Ecole Supérieure des Physique et Chimie Industrielle, the Cavendish Laboratory, the University of Grenoble. and the National Insititute for Standards and Technology. His recent research interests include fullerene solids, nanotubes. and nanowires.

* To whom correspondence should be addressed. E-mail: fischer@lrsm.upenn.edu.

10.1021/ar0101638 CCC: $22.00
Published on Web 07/10/2002

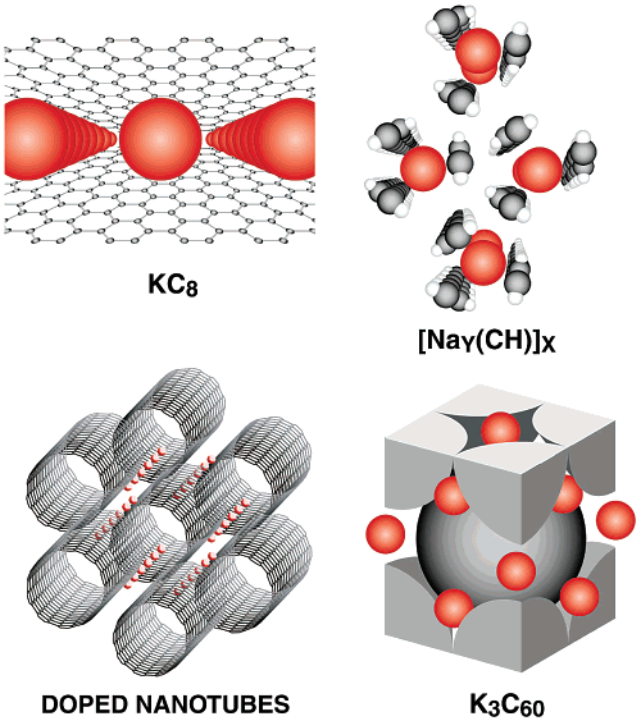

FIGURE 1. Chronology of carbon-based crystalline solids which function as hosts for chemical doping or intercalation (clockwise from upper left). The stoichiometric graphite intercalation compound KC_8 was discovered in the 1920s; it consists of alternating monolayers of graphene and potassium. The solid-solution-doped conjugated polymer $[Na_y(CH)]_x$ evolved from experiments performed in the late 1970s; the chains of neat polyacetylene rotate and expand to create one-dimensional channels which can be filled with potassium. The stoichiometric fulleride superconductor K_3C_{60} was discovered in 1991; here, the potassiums occupy the tetrahedral and octahedral sites in the face-centered-cubic van der Waals crystal formed by close-packed C_{60} molecules. Finally, a hypothetical nanotube intercalation compound was suggested by the discovery that SWNTs self-assemble into 2D trigonal crystals during growth. Adapted from ref 4; see also ref 3.

these deformations decay rapidly in the plane—the graphene sheet "conforms" to the local interlayer perturbation. This means that the local elastic potential is large, as is the associated strain dipole, leading to complete gallery filling even at low global concentration. The resulting long-period 1D superlattice, driven by interlayer repulsion, remains stable to relatively high temperature. Conversely, TiS_2 layers are stiff due to the internal S−Ti−S covalent bonds, distortions decay slowly, dipoles are weak, and the Ising transition temperature is depressed. This explains why electrochemically intercalated Li_xTiS_2 shows only the lattice gas, or disordered paramagnetic, phase at 300 K for all x, while high stages in graphite are stable to as high as 700 K, depending on concentration.[10] The analogous host deformations in polymers consist of chain rotations which open up three- or four-fold channels to accommodate the guest atomic or molecular chains.[6]

What about SWNT ropes? Nanoscale cylinders are stiffer than sheets, so elastic interactions will be weak. Similarly, rotating SWNTs about their axes affects site energies only to the extent that local commensurability

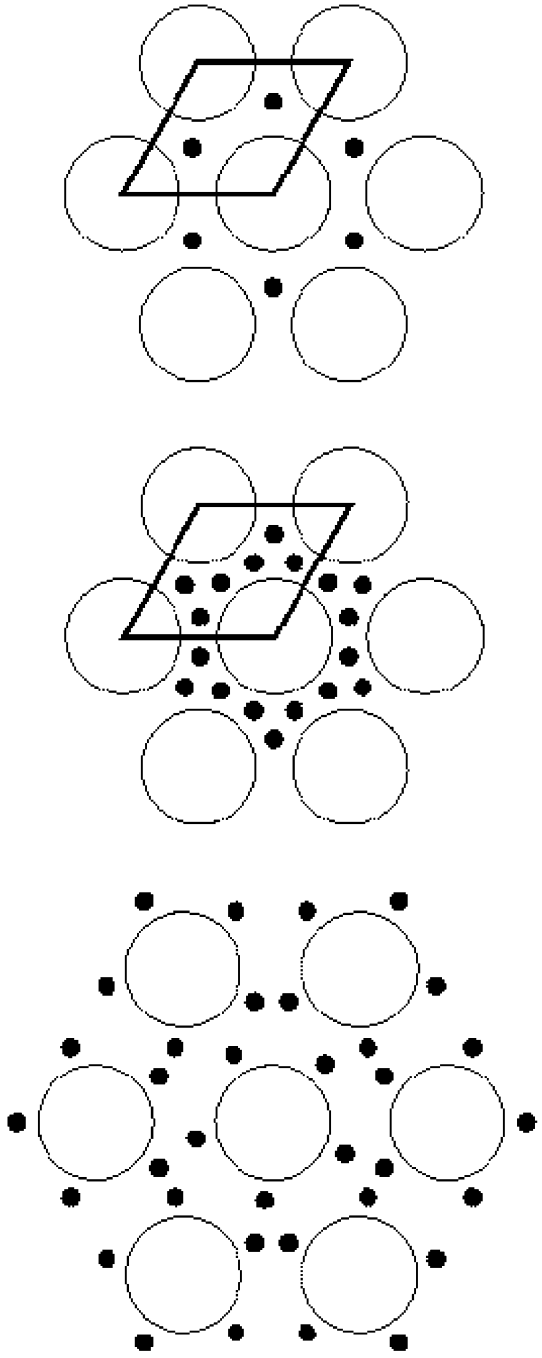

FIGURE 2. Schematic projections of hypothetical intercalation motifs for SWNT ropes. Filling the trigonal channels with close-packed ionic chains gives projected saturation compositions K:C = 1:40 and 1:13, assuming 1 and 3 chains per channel, (a) and (b), respectively. Wrapping each tube with a 2D commensurate K superlattice is formally equivalent to KC_8 graphite, as shown in (c).

with the hexagonal atomic structure on the tube walls is important. Furthermore, since the close-packed 2D lattice has three-fold rotational symmetry, only tubes with wrapping indices (n,m) *modulo* 3 can have long-range order, all others being frustrated. We therefore concluded at the outset that intercalated SWNT structures would most likely be of the lattice gas type, with variable random filling as a function of guest concentration. Furthermore, since

none of the structural energies appeared to be relevant, intercalation reactions with SWNT would necessarily involve guest−host charge transfer in order to stabilize the compounds via ionic guest−host interactions.

The search for SWNT intercalates is complicated by the nature of available materials. The crystal structure of SWNT ropes is poorly defined due to polydisperse tube diameters and chiralities, and by the limited crystallite size. Tubes and ropes bend with surprisingly small radii of curvature, so structural units of the intercalation host are not even straight beyond the scale of 100 nm or so. Bulk material is highly porous, which is advantageous for doping kinetics but certainly not for the interpretation of bulk measurements. Reasonably crystalline ropes comprise only a fraction of the total volume (sometimes zero), depending on how the soot is produced.

Early Experiments

Therefore, our first modest experiment[11] was a search for two classic signatures of redox intercalation: conductivity enhancement and at least partial reversibility. The simplest reactions to perform are those with the halogens. We know from graphite and polyacetylene that F_2 and Cl_2 are most likely to covalently attach, while Br_2, I_2, and the interhalogens IBr and ICl will intercalate from the vapor, the melt, or organic solvents. A pressed "mat" of unpurified SWNT soot was mounted in an O-ring sealed glass vessel with four hermetically sealed electrical leads and a small amount of bromine. The vessel was evacuated with the Br_2 frozen. Once the bromine was allowed to melt and vaporize, the sample resistance dropped very rapidly (minutes) by a factor of 15, an encouraging sign. Cycling was carried out by alternately freezing the bromine while heating the sample, and remelting the bromine once the sample had cooled. The results in Figure 3 indicate partial reversibility and cyclability of the doping process.

The presumptive interpretation is that delocalized electrons initially present on the SWNT were extracted, leading to p-type doping of the tubes, charge-compensated by anionic guest species, e.g., Br_2^-, analogous to graphite. This picture is much too simple. SWNT ropes and mats contain both metallic and semiconducting tubes, in relative abundance 1:3 if the tube growth mechanism is stochastic (all possible diameters and chiralities equally weighted). Thus, a somewhat better scenario is that the initially semiconducting tubes become metallic while the initially metallic ones become better metals with higher electronic density of states at the Fermi energy, $N(E_F)$.

A similar experiment with potassium vapor was carried out using vacuum line and glovebox techniques.[12] The limiting weight uptake was K:C ≈ 1:8, comparable to those of KC_8 graphite, the bcc fulleride K_6C_{60}, and alkali-doped $(CH)_x$. For an ordered structure, this would be consistent only with the wrapped 2 × 2 model (Figure 2). The fact that the maximum K:C ratios are similar for graphite and SWNT suggests that the benzenoid hexagonal network has a finite capacity to accommodate delocalized negative

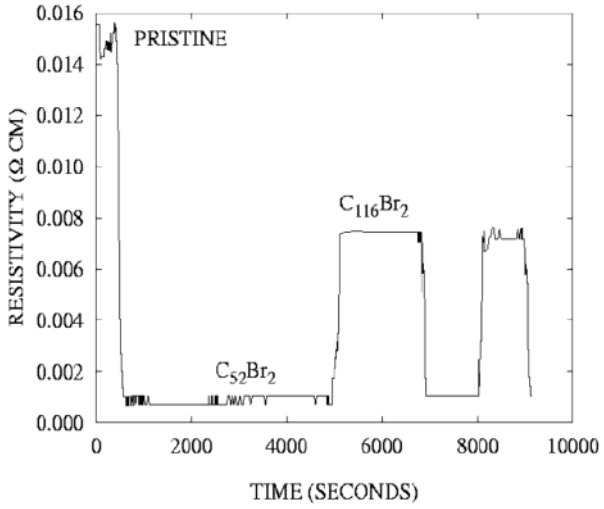

FIGURE 3. Resistance of a bulk SWNT sample vs time of exposure to Br_2 vapor at 300 K. Within minutes, *R* has dropped 15-fold; the composition (determined separately from weight uptake) is ~$C_{52}Br_2$. After 3000 s the apparatus was opened to laboratory air, with no change in *R*. After 5000 s the sample was heated in air with a heat gun, which increased *R* to about half its initial value and decreased the bromine content as shown. Re-exposing the same sample returned *R* to its previous minimum value.

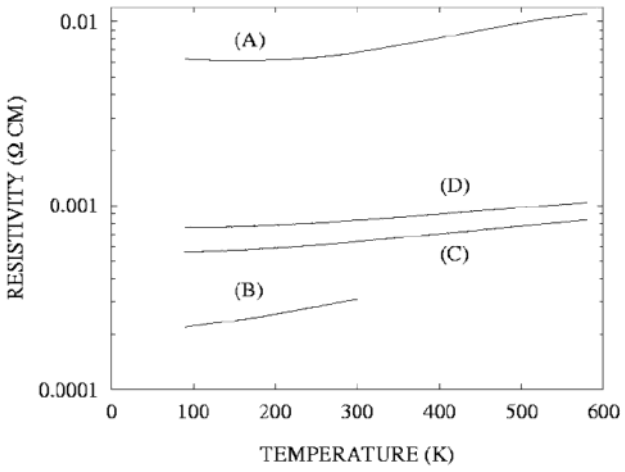

FIGURE 4. Resistivity vs temperature for a bulk SWNT sample: (A) pristine material; (B) after doping with potassium at 473 K; (C) after heating in the cryostat vacuum to 580 K overnight; (D) after 3 days at 580 K.

charge. Such a limit might be imposed by a maximum dilation of C−C bonds which accompanies the screening of σ orbitals by delocalized π electrons.[13]

The K-doped mat was mounted in the glovebox onto the coldfinger of a continuous-flow cryostat to permit four-point $R(T)$ measurements from 10 to 300 K. The results are shown in Figure 4. Saturation doping reduces *R* by a factor 40 at 300 K. After doping, dR/dT is positive at all temperatures, while the pristine mat shows a weak crossover from positive to slightly negative below ~200 K. Data for the doped sample fits the classic theory for metals: $R = A + BT^n$, where *A* represents extrinsic elastic scattering of electrons (or holes) by impurities, etc., while the power law term comes from electron−phonon scat-

tering. Alkali doping was also found to be partially reversible by heating in a vacuum, as shown.

Why should such relatively simple ideas explain the doping response of impure, porous, polydisperse, probably inhomogeneous SWNT material consisting of randomly oriented tubes and ropes? Alternative explanations could be that doping serves primarily to improve transport across interparticle contacts by reducing tunneling barriers, or to provide conducting shunts around highly defective or undoped nonconducting regions. We addressed these issues by comparing the doping response of mats and single ropes.[12] For the latter, laser-grown SWNT material was dispersed in ethanol and then dropped onto a SiO_2-coated Si substrate. Using atomic force microscopy, we selected a 35-nm-diameter rope over which four chrome-gold leads were patterned by electron beam lithography and liftoff. After completing the pristine measurements, K doping was carried out by heating the sample to 423 K, with the metal reservoir at 400 K, for 15 h.

Before doping, the scaled $R(T)$ is the same for rope and mat from 13 to 300 K, which allows us to rule out tunnel barriers between ropes as the limiting factor in the undoped mat since tunneling probabilities are generally strongly dependent on T. Similarly, the difference in absolute resistivities can be explained by invoking a longer path for the average conduction electron to traverse a given length, since many ropes will be involved in macroscopic transport. After doping, $R(T)$ for the rope closely resembles that of the mat, indicating again that the complex morphology of the rope has little influence on the electronic consequences of charge-transfer doping. The rope data also confirmed that all tubes became metallic after doping, because gate modulation of the rope conductance was completely suppressed.

In Situ Electrochemical Studies

The next challenge was to seek evidence for the hypothetical structures shown in Figure 2, or, more generally, to find out where the dopants reside. Even without staging, it would be advantageous to carry out a diffraction study as a continuous function of concentration in order to follow the filling of lattice gas sites. Again, borrowing from experience with graphite and polymers, we designed a set of in situ electrochemical experiments, which in addition would facilitate the search for definitive signatures of a metallic doped state.

Reversible electrochemical insertion of Li into SWNT was investigated by galvanostatic charge/discharge on half-cells consisting of purified SWNT buckypaper and Li metal with 1 M $LiPF_6$ in EC:DMC as electrolyte.[14] The cell (Figure 5) was equipped with a cylindrical Be window and a magnetically driven piston, which permitted raising and lowering the electrolyte level for doping/dedoping or X-ray data accumulation, respectively. The results are shown in Figure 6. The reference spectrum shows broad reflections

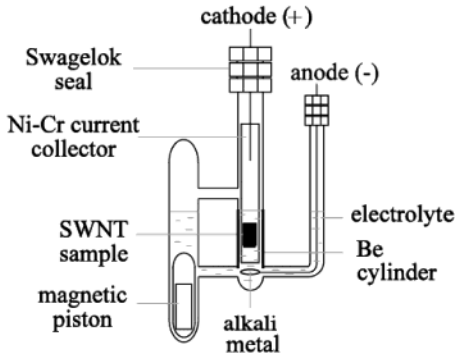

FIGURE 5. Three-arm cell for in situ X-ray diffraction under electrochemical control. Raising the magnetic piston lowers the electrolyte level, exposing the sample to the X-ray beam without absorption and diffuse scattering from the liquid.

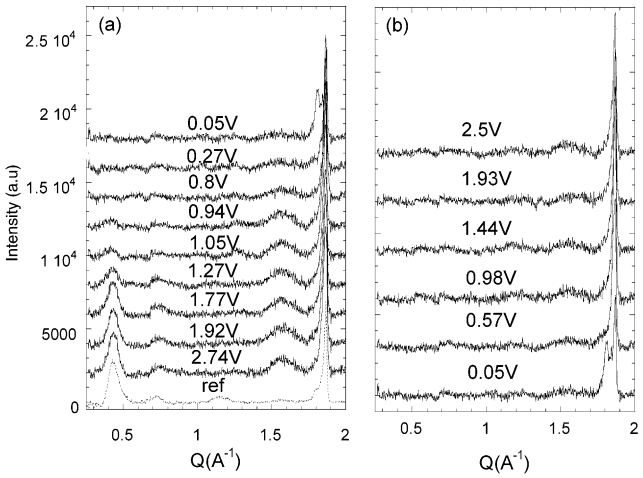

FIGURE 6. In situ powder X-ray profiles measured at fixed cell potentials during Li insertion (panel a, bottom to top) and de-insertion (panel b, bottom to top). As insertion progresses, the first-order rope peak at $Q = 0.43$ A^{-1} ($Q = 4\pi \sin\theta/\lambda$) decreases in intensity without shifting or broadening. Crystalline ropes are restored after de-insertion only after washing followed by a high-temperature anneal.

of the 2D triangular rope lattice and a sharp (002) peak from residual graphite impurity. Upon doping, we observe a progressive decrease in rope intensities with no change in position. Near maximum doping (lowest cell potential), the graphite (002) (ABAB.. stacking) evolves toward the LiC_6 (001) (AAAA.... stacking), confirming proper operation of the cell. Reversing the current (dedoping) leads to recovery of pristine graphite but not the ropes. Crystallinity could be restored by high-temperature annealing after disassembling the cell. Similar results were found with potassium;[15] here, the higher scattering power would certainly reveal lattice gas filling and/or lattice dilation. Evidently, electrochemical doping "frays" the ropes by progressive solvent co-intercalation rather than exfoliating them, since crystallinity can be restored upon removal of the electrolyte, washing, and annealing. Conversely, vapor-doped samples remain crystalline; X-ray studies show evidence for uniform dilation, but the relative intensities are still inconsistent with appreciably filled channels in the doped state.[16] A convincing fit of scattering data to

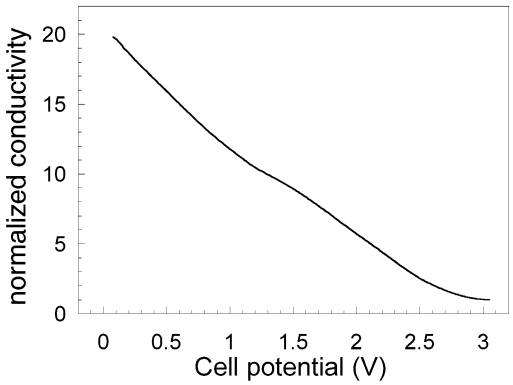

FIGURE 7. In situ four-probe conductance of Li-doped SWNT vs electrochemical potential in EC:DMC $LiPF_6$. Conductance is normalized to that of the undoped sample at 3 V.

any structural model for *any* dopant has yet to be achieved.

Having failed to solve structural issues using in situ electrochemistry, we turned to other concentration-dependent experiments which address the metallic nature of the doped state. Three separate experiments were performed in which galvanostatic potentiometry for composition control was combined with either four-point resistivity, electron paramagnetic resonance spectroscopy (EPR), or Raman spectroscopy.[15] The existence of EPR is definitive proof of a metallic state since it measures the concentration of Pauli spins, which is proportional to $N(E_F)$. Doping-induced red shifts of certain Raman-active modes are measures of the aforementioned C−C bond softening with n-doping (conversely for p-doping),[17] thus providing further proof of the existence of delocalized (metallic) electrons.

Resistance was measured as a continuous function of cell potential by using a low audio frequency lock-in arrangement to measure R without interference from the dc galvanostat. Figure 7 shows the results obtained with $LiPF_6$/EC:DMC, plotted as $G = 1/R$ vs cell potential. G increases monotonically with Li concentration from $x = 0$ (3 V) to $x = 1.4$ (~0 V) in the formula Li_xC_6. The effect is perfectly reversible (not shown). The increase is linear in cell potential but highly nonlinear in x, since most of the Li uptake occurs at potentials below 0.5 V. Most of the conductance enhancement therefore occurs in the early stages of doping, $x < 0.1$. Similar results are obtained for K doping using 1 M KCN in anhydrous $(C_2H_5)_3B$/THF. In neither case do we find evidence for anomalies or nonmonotonic behavior, which might be expected if $\mu(x)$ were to encounter an electronic singularity as x is varied.

Microwave ESR could be done only with the weakly polar KCN-based electrolyte, for which the maximum K:C ratio is limited to 1:24 since THF co-intercalates to form a partially solvated ternary compound. No conduction electron signal was detected in the undoped state. We attribute this to the presence of ~1 at. % Ni impurity, such that, at low electron density, the induced spin alignment is more likely to dephase by interacting with ferromagnetic Ni than with another electron. A well-defined line emerged upon doping; its intensity increased monotonically with

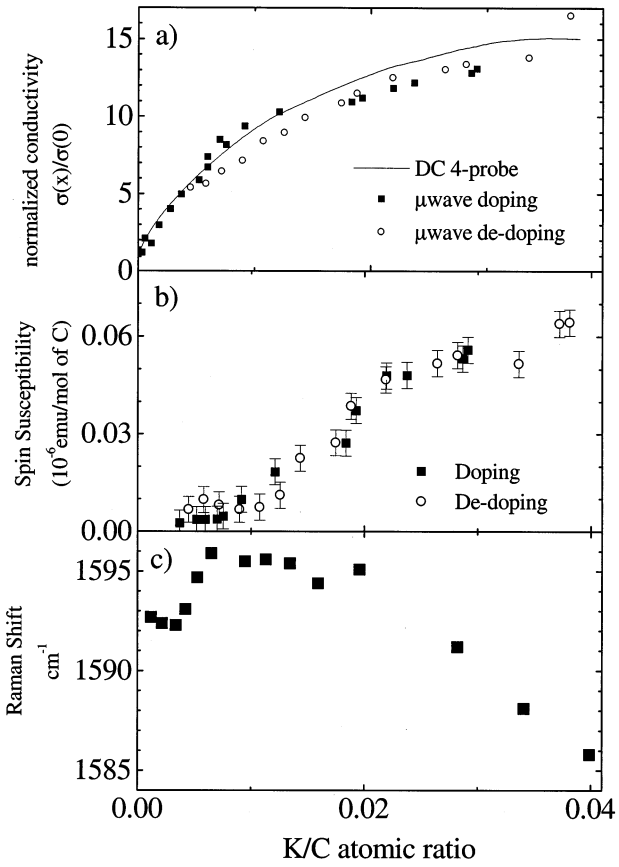

FIGURE 8. In situ measurements of electrical conductivity (a), spin susceptibility (b), and shift of the Raman-active tangential G-band (c) as functions of K:C ratio during galvanostatically controlled insertion and de-insertion. The maximum K:C is limited by co-insertion of THF solvent. Panel a shows that the conductivity enhancement saturates at K:C ≈ 0.04, is completely reversible (solid and open circles), and is the same measured at microwave and low audio frequencies. Panel b shows that the spin susceptibility also evolves reversibly with K concentration, more rapidly above K:C = 0.007. Panel c shows that the Raman shift, a signature of charge transfer, also evolves continuously (and reversibly, not shown) and exhibits nonmonotonic behavior below K:C = 0.007.

increasing K:C, but the line width and position remained constant. The Pauli susceptibility χ_P, proportional to $N(E_F)$, is plotted vs K:C ratio in Figure 8b. Despite the large error bars, there appears to be an induction period below K:C ≈ 0.007, above which χ_P increases rapidly. It is perhaps more convincing to extrapolate back from large χ_P and note the positive intercept at $\chi_P = 0$. While reminiscent of the soliton doping regime in polyactylene (large conductivity enhancement with no spins), the effect in polydisperse SWNT most likely represents the K concentration at which all the semiconducting tubes are doped into the metallic regime. A similar anomaly is observed in the Raman shift vs K:C, Figure 8c. Above K:C = 0.007, a continuous and reversible red shift is observed due to charge-transfer-induced softening of the C−C bonds, consistent with the concomitant increases in conductivity (Figure 8a) and χ_P. At lower K:C, the shift is not monotonic, precisely in the range where χ_P depends only weakly on K:C.

The doping-induced enhancement in χ_P is fully reversible, and χ_P is independent of temperature from 20 to 300 K, characteristic of a metal. The absolute value at K:C = 0.04 is 5×10^{-8} emu/g, from which $N(E_F) = 0.015$ states per electronvolt per spin, about 5 times smaller than a theoretical estimate for tubes with an appropriate diameter distribution doped with 1 electron per 24 carbons. This discrepancy may be due in part to solvation effects, i.e., less than 1 delocalized electron per K.

More significant is the fact that the line width is independent of K:C, which is not consistent with the standard picture of EPR for uniform Pauli spins in a metal. The usual mechanism for spin-relaxational line broadening in guest−host systems is spin−orbit scattering by the dopants, which increases strongly with atomic number and depends sensitively on the electronic structure. If the doping were homogeneous, the line width would increase with increasing K concentration. An explanation consistent with the X-ray results would be a two-domain picture of K-saturated domains embedded in undoped regions. Now the EPR signal becomes a coupled resonance of undoped and doped domains, dominated by the latter since their contribution is weighted by a much larger value of χ_P, even at small K:C ratios. Inhomogeneous doping increases the number and/or size of K-saturated domains without changing their electronic structure; thus, the line width is independent of the global K:C ratio, except at extremely low concentrations. The ESR intensity is now proportional to the volume fraction of saturation-doped domains, which explains the quasi-linear dependence of χ_P on the K:C ratio. The spin relaxation rate is constant because $N(E_F)$ in the domains is independent of K:C.

The choice of "two-domain" rather than "two-phase" terminology is deliberate, because we believe the domains represent a form of quenched disorder. In general, a two-phase model implies one or more first-order transitions vs chemical potential (or global concentration), as one well-defined phase grows at the expense of another. No evidence of such transitions is found in cyclic voltammetry (CV) or charge/discharge (CD) experiments, which we attribute to the intrinsic disorder and nanoscopic length scale of the doped and undoped regions. Both kinds of domain consist of tubes with different diameters, chiralities, and lengths, such that there is no well-defined K-site binding energy. Furthermore, the small domain size is probably of the same order as the width of the domain walls, such that doped and undoped regions cannot be viewed as independent objects which merely exchange dopants with each other. We therefore expect a wide distribution of redox potentials such that redox peaks in cyclic voltammetry and plateaus in galvanostatic charge/discharge are completely washed out, as observed.

The growth of fully doped domains at the expense of undoped crystalline material is consistent with the evolution of X-ray profiles vs K:C, in particular the observation that rope intensities decrease but do not not shift with K:C. We envisage K^+ ions, perhaps solvated by THF, invading the van der Waals channels between adjacent tubes in a rope, but in a disordered arrangement which precludes the existence of intercalation superlattices. Alternatively, small-diameter ropes could be fully doped, while larger ones remain undoped or partially doped due to slow diffusion kinetics. Analogous line splitting was not observed in the Raman spectra, most likely because the Raman line broadened with doping such that any unshifted contribution from undoped domains was obscured. The broadening of Raman lines with increasing delocalized electron density is well-represented by a Breit−Wigner−Fano resonance between a discrete molecular vibration and an electronic continuum,[17] as in GICs.

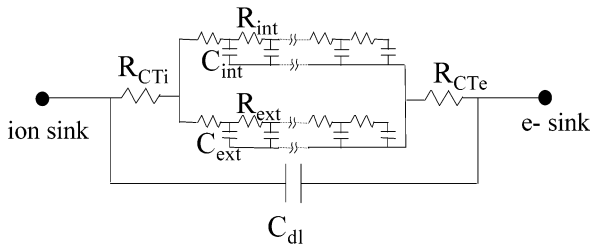

FIGURE 9. Equivalent circuit used to model electrochemical impedance spectra for Li- and K-doped SWNT. The two transmission lines in parallel represent the internal and external diffusion processes in and around an average SWNT rope in porous bulk material. Charge-transfer resistance is split into ionic and electronic components to allow for charge-transfer doping of the working electrode. All of this is shunted by the usual double-layer capacitance of the macroscopic solid/liquid interface.

Further support for the two-domain model of electrochemically doped SWNT comes from electrochemical impedance spectroscopy (EIS),[18] which measures the frequency-dependent complex impedance of an electrochemical cell as a function of cell potential, the latter being directly related to the dopant concentration. Using equivalent circuits to model the data, one obtains parameters relating to the kinetics and energetics of the doping process. The best fit to EIS data for K- and Li-doped SWNT was obtained using the equivalent circuit shown in Figure 9. Charge-transfer resistance at the electrode−electrolyte interface is split into ionic and electronic terms, the latter varying with cell potential as the SWNT working electrode is doped and undoped during cycling. The two RC transmission lines in parallel represent fast diffusion through the mesoscale porosity of the electrode and slow nanoscale diffusion in individual SWNT ropes.

For both alkalis, fitted EIS values of electrode resistance and storage capacitance compare very well with direct dc measurements. For example, Figure 10a compares R_{ct} with four-point resistance, both vs cell potential, for Li/SWNT. The former can be interpreted as a constant ~100 Ω ionic contribution plus an electronic term which decreases with doping ($V > 0$), similar to the directly measured resistance (the different absolute values are due to different electrode geometries). Similarly, in Figure 10b, we see that the sum of the two EIS diffusion capacitances matches the directly measured cell capacitance obtained by differentiating a charge/discharge curve. The significance of this equivalence is that the galvanostatic capacity is entirely accounted for by Li intercalation.

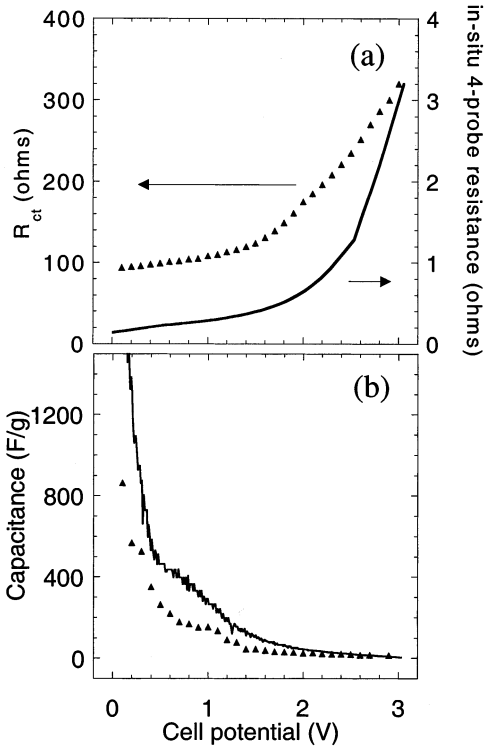

FIGURE 10. (a) Charge-transfer resistance vs cell potential (filled triangles) for Li/SWNT, compared with bulk electronic resistance of a similar electrode measured in situ using four-probe resistivity (solid curve). (b) SWNT capacitance as a function of cell potential. Filled triangles are the EIS results ($C_{ext} + C_{int}$), while the solid curve was derived from galvanostatic measurements using $C = dQ/dV$.

The time constant for rapid diffusion decreases from 70 to 7 s as the global concentration increases from zero to its maximum value $Li_{1.4}C_6$, while the slower process proceeds with about the same 2500 s time constant throughout the cycle. We expected quite the opposite behavior in our initial premise; the rate of fast diffusion through mesopores should not vary with cell potential unless the morphology changes during cycling, while slow diffusion within ropes should accelerate as the ropes lose crystallinity by "fraying". We believe that these discrepancies can be attributed to the electrolyte solvent. Swelling of the electrode to a gel-like state would certainly speed up M^+ diffusion through the pores (as in gel electrolytes), while the diffusion rate of solvated M^+ is likely to be dominated by the bulky solvent molecule at all concentrations, even after the ropes become "frayed". It would certainly be useful to repeat these experiments with a nonsolvating electrolyte system and/or on SWNT electrodes with known and controllable microstructure and porosity.

Summary and Prospects

Our findings to date on intercalated SWNT can be summarized as follows. Reversible charge-transfer doping which leads to a metallic state for bulk SWNT is firmly established for both electrochemical and direct vapor/liquid methods. Conductivity enhancements as large as 40 times can be achieved at 300 K on bulk samples and single ropes, comparable to GICs but less dramatic than fullerides or conjugated polymers. The advantages of electrochemical methods for studying the basic science are offset by solvent effects which destroy crystallinity, limit the maximum dopant concentration in some cases, and obscure the dynamics of doping and dedoping. X-ray diffraction on vapor-doped samples reveals the expected dilation of the 2D rope lattice, but the intensity profiles do not come close to accounting for the weight uptake. Therefore, some degree of disorder in doped SWNTs appears to be universal. This may change as better materials become available.

All-nanotube fibers can be produced by extruding a suspension through an orifice into a liquid and subsequent drying.[19] To the extent that this process can be developed to yield long, high-strength fibers consisting of well-aligned SWNT, it would obviously be important to try enhancing their conductivity by intercalation. Interest in Li-intercalated nanotubes as candidate anode materials for Li ion batteries remains high. Li capacities more than twice as large as that of graphite have been reported on SWNT materials which have been processed to give access to the interior tube volume.[20] Several major issues remain to be resolved: unacceptably high irreversible capacity attributable to parasitic surface reactions (exacerbated in these highly porous materials), large hysteresis between charge and discharge, and large variation in anode potential vs Li/Li^+ from fully charged to discharged states. An early report that hydrogen storage capacity is enhanced by first intercalating the tubes with alkali metal has since been proven to be an experimental artifact. Exposure of a 200−500-nm length of a semiconducting SWNT to K vapor produces a single-electron transistor, or quantum dot, which is switchable between on and off states by ~2 V applied to a back-gate electrode.[21]

Intercalation chemistry generally refers to the targeting of interstitial sites in a more or less well-defined lattice without changing the structure and internal bonding of the host motif. Other nanotube chemistries are clearly possible. Accounts in this issue by Haddon and Sun deal with reactions involving tube ends (open or closed) and sidewalls. Another possibility alluded to above is filling the interior annulus. The ends of multiwall tubes can be opened by oxidation, and the annulus is large enough to permit uptake of low-surface-tension liquids by capillary forces.[22] Inorganic single crystals can be grown inside suitably prepared nanotubes from molten salt or oxide precursors.[23] SWNT can be abundantly filled with C_{60}, higher fullerenes, and endofullerenes by first etching holes into the sidewalls.[24] It would be extremely important to extend the rational synthesis of tube filling to functional molecules of biological interest.

This Account is largely based on the Ph.D. dissertations of Agnes Claye, Roland Lee, and Norbert Nemes, whose work was supported respectively by the National Science Foundation MRSEC Program Grant No. NSF DMR00-79909, U.S. Department of Energy Grant No. DOE DEFG02-98ER45701, and NSF Grant No. DMR97-30298.

References

(1) Iijima, S. Helical microtubules of graphitic carbon. *Nature* **1991**, *354*, 56−59.
(2) Thess, A.; Lee, R. S.; Nikolaev, P.; Dai, H.; Petit, P.; Robert, J.; Xu, C.; Lee, H.; Kim, S. G.; Colbert, D. T.; Scuseria, G.; Tomanek, D.; Fischer, J. E.; Smalley, R. E. Crystalline ropes of metallic carbon nanotubes. *Science* **1996**, *273*, 483−487.
(3) Fischer, J. E. Storing energy in carbon nanotubes. *Chem. Innovation* **2000**, *30*, 21−27.
(4) Fischer, J. E.; Bernier, P. Les cristaux de fullerène. *La Recherche* **1993**, *250*, 46−55.
(5) Fischer, J. E.; Claye, A. S.; Lee, R. S. Crystal chemistry of nanotube lattices. *Mol. Cryst. Liq. Cryst.* **2000**, *340*, 737−741.
(6) Heiney, P. A.; Fischer, J. E.; Djurado, D.; Ma, J.; Chen, D.; Winokur, M. J.; Coustel, N.; Bernier, P.; Karasz, F. J. Channel structures in alkali-doped conjugated polymers: broken-symmetry intercalation lattices. *Phys. Rev. B* **1991**, *42*, 2507−2515.
(7) Yildirim, T.; Zhou, O.; Fischer, J. E.; Bykovetz, N.; Strongin, R. M.; Cichy, M.; Smith, A. B., III; Lin, C. L.; Jelinek, R. Intercalation of clusters into a fullerene lattice. *Nature* **1992**, *360*, 68−70.
(8) Safran, S. A. Staging in layer intercalates. *Solid State Phys.* **1987**, *40*, 183−201.
(9) Ma, J.; Choi, H.-Y.; Mele, E. J.; Fischer, J. E. Staging in doped polymers. *Synth. Met.* **1998**, *27*, A75−A81.
(10) Fischer, J. E.; Kim, H. J. Elastic effects in intercalation compounds. *Phys. Rev. B* **1987**, *35*, 3295−3298.
(11) Lee, R. S.; Kim, H. J.; Fischer, J. E.; Thess, A.; Smalley, R. E. Conductivity enhancement in K- and Br-doped nanotube bundles. *Nature* **1997**, *388*, 255−257.
(12) Lee, R. S.; Kim, H. J.; Fischer, J. E.; Lefebvre, J.; Radosavljevic, M.; Hone, J.; Johnson, A. T. Transport properties of a potassium-doped carbon nanotube rope. *Phys. Rev. B* **2000**, *61*, 4526−4529.
(13) Pietronero, L.; Straessler, S.; Horsch, P. Charge transfer and bond dilation in graphite intercalation compounds. *Mol. Cryst. Liq. Cryst.* **1982**, *83*, 1243−1248.
(14) Claye, A. S.; Fischer, J. E.; Huffman, C. B.; Rinzler, A. G.; Smalley, R. E. Solid-state electrochemistry of the Li-carbon nanotube system. *J. Electrochem Soc.* **2000**, *147*, 2845−2852.
(15) Claye, A. S.; Nemes, N. M.; Janossy, A.; Fischer, J. E. Structure and electronic properties of potassium-doped single wall carbon nanotubes: in-situ electrochemical studies. *Phys. Rev. B* **2000**, *62*, R4845−R4848.
(16) Nemes, N. M.; Fischer, J. E., unpublished.
(17) Rao, A. M.; Eklund, P. C.; Bandow, S.; Thess, A.; Smalley, R. E. Evidence for charge transfer in doped carbon nanotube bundles from Raman scattering. *Nature* **1997**, *388*, 257−259.
(18) Claye, A. S.; Fischer, J. E.; Metrot, A. Kinetics of alkali insertion in SWNT: an electrochemical impedance spectroscopy study. *Chem. Phys. Lett.* **2000**, *330*, 61−67.
(19) Vigolo, B.; Penicaud, A.; Coulon, C.; Sauder, C.; Pailler, R.; Journet, C.; Bernier, P.; Poulin, P. Macroscopic fibers and ribbons of oriented carbon nanotubes. *Science* **2000**, *290*, 1331−1334.
(20) Shimoda, H.; Gao, B.; Tang, X. P.; Kleinhammes, A.; Fleming, L.; Wu, Y.; Zhou, O. Lithium intercalation into opened SWNT: storage capacity and electronic properties. *Phys. Rev. Lett.* **2002**, *88*, 015502-1−015502-4.
(21) Kong, J.; Cao, J.; Dai, H. Chemical profiling of single nanotubes: intramolecular p-n-p junctions and on-tube single-electron transistors. *Appl. Phys. Lett.* **2002**, *80*, 73−75.
(22) Dujardin, E.; Ebbesen, T. W.; Hiura, H.; Tanigaki, K. Capillarity and wetting of carbon nanotubes. *Science* **1994**, *265*, 1850−1853.
(23) Meyer, R. R.; Sloan, J.; Dunin-Borkowski, R. E.; Kirkland, A. I.; Novotny, M. C.; Bailey, S. R.; Hutchison, J. L.; Green, M. L. H. Discrete atom imaging of one-dimensional crystals formed within single-walled carbon nanotubes. *Science* **2000**, *289*, 1324−1327.
(24) Smith, B. W.; Luzzi, D. E. Formation mechanism of peapods and coaxial tubes. *Chem. Phys. Lett.* **2000**, *321*, 169−174.

AR0101638